

Project Tanagra: A Spectro-Temporal Stellar Events Database

Jennifer Posson-Brown (SAO/CfA), Vinay L. Kashyap (SAO/CfA), Jeremy J. Drake (SAO/CfA), Steven H. Saar (SAO/CfA), and Jeffrey D. Scargle (NASA Ames)

Summary

We describe Project Tanagra (Timing Analysis of Grating Data, <http://hea-www.harvard.edu/tanagra>), a database of temporal products obtained from archival *Chandra* gratings observations of stars. The high spectral resolution dataset consists of X-ray bright, active low-mass coronal stars which were peer-selected to be interesting. We present an introduction to *Chandra* gratings data, and discuss our analysis methods and techniques for identifying events. Grating-dispersed events are ideal for timing analysis. Advantages to using these datasets are: first, the dispersed events are generally free from pileup; second, detailed wavelength-filtered timing analysis can be performed; third, the simultaneous gathering of independent datastreams allows for a strong test of variability; and fourth, the observations span long durations and thus provide a long baseline for analysis. We plan to conduct a comprehensive and uniform analysis of all selected datasets, and make an atlas of detected events available online.

This work is supported by CXC NASA contract NAS8-39073 and Chandra grant ARO-11001X.

I. The Dataset

The *Chandra* X-Ray Observatory has two transmission gratings: the High Energy Transmission Grating (HETG), typically used with the spectroscopic array of the Advanced CCD Imaging Spectrometer (ACIS-S), and the Low Energy Transmission Grating (LETG), which can be used with the High Resolution Camera spectroscopic array (HRC-S) or with ACIS-S. The HETG consists of two sets of gratings – the Medium Energy Grating (MEG) and the High Energy Grating (HEG) – while the LETG is a single grating, the Low Energy Grating (LEG). *Chandra* grating parameters are given in Table 1, and an image of an ACIS-S/HETG observation of M1Ve star AU Mic is shown in Figure 1.

Chandra gratings observations produce photon lists, giving the arrival time, location, energy, and other parameters for each observed photon which passes the on-board filtering. The intrinsic energy resolution of ACIS-S allows for the separation of different grating orders, but this is not possible with the HRC-S, which is a microchannel plate (MCP) detector.

Chandra's observing program is chosen by yearly peer-review. From the *Chandra* archive of targets (peer-selected to be the most interesting), we choose observations of X-ray bright, active low-mass coronal stars, giving us a list of over 60 targets. The high timing and energy resolution of *Chandra* gratings data, and presence of multiple independent data streams due to the different grating arms, allows us to analyze this rich and unique dataset in new ways: examining, for example, the time variability of a given spectral line, or looking for simultaneous events in multiple data streams.

	LEG	MEG	HEG
Wavelength Range	1.2 - 60 Å (with ACIS-S) 1.2 - 175 Å (with HRC-S)	2.5 - 31 Å	1.2 - 15 Å
Resolution ($\Delta\lambda$, FWHM)	0.05 Å	0.023 Å	0.012 Å
Effective Area (1st order)	4 - 200 cm ² (with ACIS-S) 1 - 25 cm ² (with HRC-S)	7 - 200 cm ²	7 - 200 cm ²
Temporal Resolution	2.85 ms - 3.24 s (with ACIS-S, depending on mode) 10 ms (HRC-S default mode), 16 μ s (HRC-S Timing Mode)	2.85 ms - 3.24 s	2.85 ms - 3.24 s
Typical Background	<< 0.01 cts/pixel/100-ks (with ACIS-S, order-sorted) ~10 (25) cts/0.07-Å/100-ks @ 50 (175) Å (with HRC-S, after filtering)	~0.03 - 0.2 cts/Å/ks/6"	~0.1 - 0.3 cts/Å/ks/6"

Table 1 Chandra gratings parameters, from the Proposers' Observatory Guide (<http://cxc.harvard.edu/proposer/POG>), Chapters 8 & 9

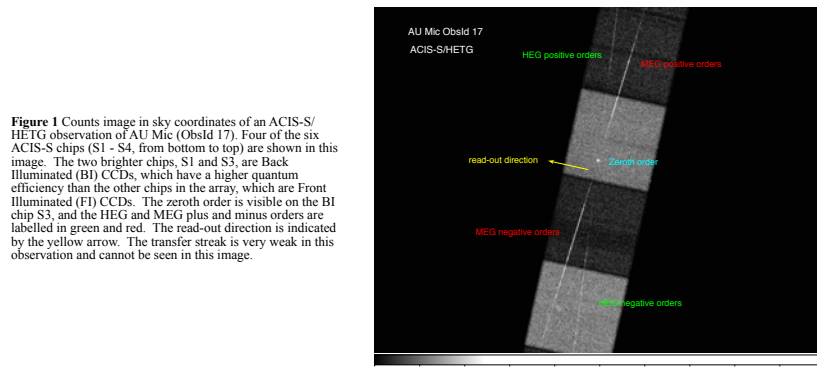


Figure 1 Counts image in sky coordinates of an ACIS-S/HETG observation of AU Mic (Obsid 17). Four of the six ACIS-S chips (S1 - S4, from bottom to top) are shown in this image. The two brighter chips, S1 and S3, are Back Illuminated (BI) CCDs, which have a higher quantum efficiency than the other chips in the array, which are Front Illuminated (FI) CCDs. The zeroth order is visible on the BI chip S3, and the HEG and MEG plus and minus orders are labelled in green and red. The read-out direction is indicated by the yellow arrow. The transfer streak is very weak in this observation and cannot be seen in this image.

II. Data Analysis & Reduction

After downloading the photon lists and other data products from the *Chandra* archive, we reprocess them with the latest CIAO/CALDB version to ensure that the most recent calibration is applied. We then extract source and background photons from the dispersed spectra and zeroth order, and, where applicable, from the transfer streak.

Next, we make counts and flux lightcurves for the broadband wavelength range and for strong spectral lines. This allows us to compare line flux changes to variations in overall luminosity. Figures 2-4 show an example of ACIS-S/HETG spectra, broadband lightcurves, and line flux lightcurves for the M1Ve star AU Mic.

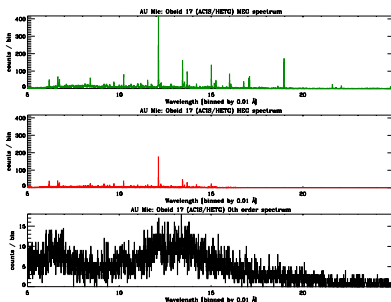


Figure 2 Background-subtracted spectra for AU Mic, ACIS-S/HETG Obsid 17, from MEG (top), HEG (middle), and zeroth order (bottom).

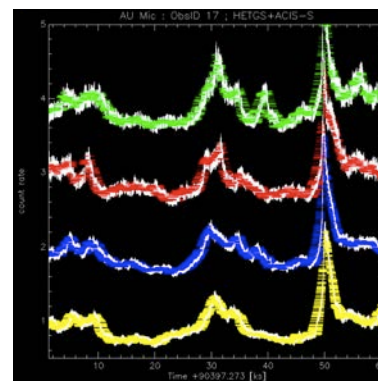
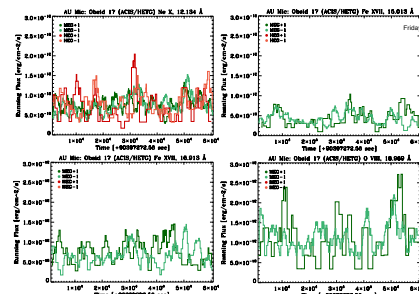


Figure 3 Background-subtracted running mean lightcurves, with ~ 50 independent bins, for AU Mic, ACIS-S/HETG Obsid 17, from dispersed first order events. Each lightcurve is normalized to its mean value, and the top three lightcurves are offset for clarity. The vertical bars denote statistical 1 sigma error, and the horizontal bars denote the time range over which the mean rate is calculated. Shown from top to bottom are HEG +1 (green; offset by +3), HEG -1 (red; offset by +2), MEG +1 (blue; offset by +1), and MEG -1 (yellow).

Figure 4 Background-subtracted running flux lightcurves for specific lines in the AU Mic dispersed spectrum (ACIS-S/HETG Obsid 17). Top: Ne X at 12.134 Å (left), Fe XVII at 15.013 Å (right). Bottom: Fe XVII at 16.913 Å (left), O VIII at 18.969 Å (right).

III. Identifying Events

To detect and characterize statistically significant local variability ("events") in the *Chandra* grating lightcurves, we use the nonparametric *Bayesian Blocks* algorithm developed by Jeffrey Scargle (<http://arxiv.org/pdf/1207.5578v3.pdf>). This algorithm finds the optimal segmentation of the data, with the beginning and end of each block marked by a change-point: a time at which the lightcurve's statistical properties change. Within each block, the lightcurve is constant within statistical errors. Thus, the *Bayesian Blocks* model for the lightcurve is defined by the number of change-points (or number of blocks, which will be one more than the number of change-points), the starting time of each block, and the lightcurve value (count rate intensity) in each block.

An event is identified by searching for local maxima at the coarse resolution of the combined data, then follow-up analysis is done at finer resolution and for the separate data streams. Change-points are checked across data streams, and those that coincide in multiple streams (as in the following example) are followed up with wavelength-filtered analysis, focused on specific lines. Figure 5 shows the AU Mic lightcurves from each HETG arm/order (top four panels), and transfer streak and zeroth order (bottom two panels), with segments shown in red. Note that all lightcurves except the transfer streak show a bright event occurring simultaneously just before the 9.045×10^7 second mark. Figure 6 shows segmented lightcurves from the combined dataset with different prior distributions chosen for the number of blocks in the two panels, adjusting the sensitivity of the algorithm.

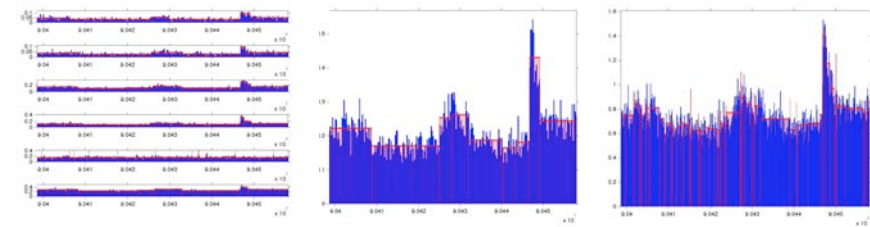


Figure 5 AU Mic lightcurves (ACIS-S/HETG Obsid 17); the top four panels are dispersed events from the plus and minus HEG/MEG first orders, and the bottom two panels are transfer streak and zeroth order events. The Bayesian Blocks model is shown in red. Note that all data streams except for the (weak) transfer streak show a simultaneous event occurring shortly before time= 9.045×10^7 seconds.

Figure 6 The combined lightcurve, in blue, with the Bayesian Block model shown in red. In the right panel, a larger number of change-points were allowed, resulting in a finer segmentation of the lightcurve compared to the left panel.

IV. Simultaneous Events

Chandra gratings observations give us the opportunity to analyze multiple independent data streams from a single observation: four dispersed grating/order arms, plus zeroth order and transfer streak data in the case of ACIS-S/HETG; two dispersed orders (+/- 1), zeroth order, and transfer streak data in the case of ACIS-S/LETG; and two dispersed orders plus zeroth order data in the case of HRC-S/LETG. The multiple data streams present an advantage when detecting events in the lightcurves: it is easier to pick up weak real events and to filter out random noise fluctuations. If an event is seen simultaneously in multiple data streams, we can be more confident that it is a real event and not a statistical fluctuation. Table 2 demonstrates via simulations that a joint analysis of two simulated data streams will result in fewer false positives than an analysis where the two streams are co-added prior to event detection.

k	1	1.5	2	2.5	3
$\mathcal{N}(\cdot)$	0.16	0.067	0.022	0.006	0.0013
$< \mathcal{N}(\cdot) \mathcal{N}(\cdot) >$	0.025	0.0045	0.0005	0.0004	$8 \cdot 10^{-7}$
$\mathcal{N}(\cdot) + \mathcal{N}(\cdot)$	0.078	0.017	0.002	0.00015	10^{-5}
$\mathcal{N}(\cdot)^2$	0.025	0.0045	0.0005	0.0005	$4 \cdot 10^{-6}$

Table 2 Type I error (fraction of fluctuations that exceed $k\sigma$) for Gaussian fluctuations from simulations. Note that analyzing the data jointly (second row) gives lower false positive rates than co-adding the data (third row). These results are based on 10000 simulations of streams with no events, but with Gaussian noise added. Work to extend these results to the Poisson case is underway. It should be noted that this determines the Type I false positive rate, but not the Type II false negative rate. Thus, this is a tool that can be used to eliminate more statistical fluctuations from the database of events, but cannot as yet be used to find weaker events.

References

- Kashyap, V.L., Sarr, S., Drake, J.J., Reeves, K., Posson-Brown, J. & Connors, A., 2011, SCMA V, http://astrostatistics.psu.edu/su11scmas5/lectures/kashyap_scma_poster.pdf
- Posson-Brown, J. & Kashyap, V.L., 2011, AAS, 21822801P
- Scargle, J.D., Norris, J.P., Jackson, B. & Chiang, J., 2012, arXiv:1207.5578v3

